nzsee
NEW ZEALAND SOCIETY FOR EARTHQUAKE ENGINEERING

Numerical parametric analysis of gravity column base-plate connections

J.C.W. He, G.C. Clifton
Department of Civil and Environmental Engineering, University of Auckland, Auckland.

S. Ramhormozian
Department of Built Environment Engineering, Auckland University of Technology, Auckland.

ABSTRACT

Gravity column base-plate connections are normally treated as pinned connections in design. Correspondingly, a low rotational stiffness value is specified in the New Zealand Steel Design Standard, NZS 3404. However, previous experimental and numerical studies have shown that these pinned connections are significantly stiffer than the recommendation in NZS 3404. Such unexpected rotational stiffness may lead to yielding at the bottom of the column. If this happens, the pre-existing axial compression load could potentially facilitate the occurrence of column axial shortening under yielding, which is difficult and costly to repair. Motivated by the observed discrepancy in column base rotational stiffness and the undesired consequences, a numerical parametric study has been conducted to determine the accurate rotational stiffness for gravity column base-plate connections, as well as to investigate the influence on the stiffness of various parameters, including the base plate thickness, anchor rod diameter, axial load ratio, foundation depth and anchor rod pitch distance.

The results agree with already published studies and further confirm the fact that the NZS 3404 requirement underestimates the rotational stiffness of gravity column base-plate connections. It has also been found that the axial load ratio and column flange slenderness ratio has the most prominent effect on the connection behaviour. Results from an ongoing work, which investigates the susceptibility of gravity columns to axial shortening, are also presented. These more detailed studies are showing that non-compact gravity columns loaded with high compressive axial load could result in severe local buckling and axial shortening under reversed cyclic loading.

1 INTRODUCTION

Column base-plate connections are critical components in a steel-framed structure due to their influence on the performance of the whole structure as well as the inelastic demands of individual structural components. Based on the rotational stiffness provided by the column base-plate detail, traditional design procedure classifies column bases into either "Pinned" or "Fixed" bases, where the column bases are assumed to possess zero or infinite stiffness, respectively. Specifically, "Pinned" column bases are usually used in gravity systems where "Fixed" column bases are often used in seismic resisting systems. However, past studies have shown that such simplification is inaccurate and could lead to high analysis error and potential structural failures (Borzouie et al., 2016; Inamasu et al., 2018; Zareian & Kanvinde, 2013). Recognizing these issues, the New Zealand Steel Structures Standard (1997), NZS3404, recommends a rotational stiffness value of $1.67EI/L$ and $0.1EI/L$ for "fixed" and "pinned" conditions, respectively, in which E, I and L are respectively the elastic modulus, second moment of area and ground floor column height. Although these values aim to represent the realistic condition in practice, they still proved to be inaccurate. Reconnaissance of the 2010/2011 Christchurch earthquake series revealed that the column base-plate connections for seismic resisting columns may be more flexible than expected as there was no observation or record of column base yielding despite the strong ground motion (Clifton et al., 2011; Clifton & MacRae, 2013; Clifton, 2013; Clifton et al., 2012; MacRae et al., 2015). On the other hand, experimental and numerical findings have shown that "pinned" column base-plate connections are considerably stiffer than the value outlined in NZS 3404 (Nawar et al., 2021; Pan et al., 2021; Picard & Beaulieu, 1985). On first sight, it may seem that the stiffer behaviour is beneficial as it provides additional stiffness to the structure. However, it also means that the connection could attract greater moment and eventually yield the column at the base. Once the column is yielded, the constant applied axial load and reversed loading can facilitate the occurrence of column axial shortening, which increases the difficulty and cost of post-earthquake rehabilitation.

Motivated by the concerns mentioned above, a finite element numerical study was conducted in ABAQUS/CAE (Smith, 2021) to determine the accurate rotational stiffness for gravity column base-plate connections (i.e., pinned connections). In addition, this study investigates the influences of various parameters, including the base plate thickness, anchor rod diameter, axial load ratio, foundation depth and rod pitch distance, on the connection behaviour. Finally, results from ongoing work which focuses on the cyclic behaviour of the connection are also presented.

2 ADOPTED CONNECTION AND CONSIDERED PARAMETERS

Figure 1 shows the configuration of the gravity column base-plate connection considered in this study. It should be noted that most the figures and table shown in this paper are taken from a published paper that was written by the same first author (He et al., 2023). A 310UC 118 column section was used, as it represents the typical column size for a low-to-medium height steel-framed structure. The column height adopted in this study was 2.52 m, which reflects the column inflection point being at 0.6L from the column base where L = 4.2 m. The base plate welded to the bottom of the column is 400 × 400 mm in size. The grout layer underneath has the same dimensions as the base plate and has a thickness of 50 mm. Levelling nuts and washers were also modelled as they are commonly used in practice for column erection. The dimensions of the concrete foundation (i.e., 2 × 2 m) were selected such that the boundary effects were minimized. Past earthquake reconnaissance and studies have shown that soil can provide additional flexibility to the column base-plate connection and affect its response (Borzouie et al., 2016; Clifton, 2013; Zareian & Kanvinde, 2013). However, this study focuses on the connection behaviour itself and the inclusion of soil flexibility is outside the scope of this study but is within the scope of this overall project.

Table 1 summarizes the considered parameters and their corresponding values. It should be noted that the applied axial load in the finite element analysis (i.e., earthquake load case $G + Q_c$ where G is the dead load and Q_c is the live load modified by the load combination factor) were back calculated from the gravity column design load (i.e., load case $1.2G + 1.5Q$) taken as 80% and 50% of the column design section capacity (ϕN_s). For naming purposes, the name of each configuration will be consisted of symbols representing the parameters followed by the corresponding values. For example, 310UC118-t25d16N40D1p100 represents that the connection has a 310UC118 column section, a 25 mm thick base plate, four 16 mm anchor rods (4 rods are used in all cases so the number doesn't appear in the designation), applied with an axial load equivalent to 40%ϕN_s, a 1 m deep foundation and a 100 mm anchor rod pitch distance.

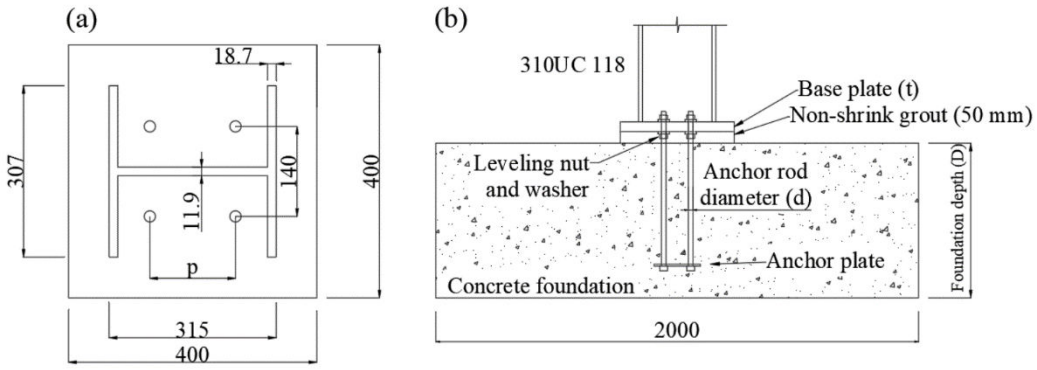

* All dimensions in mm. Some dimensions are not shown as they are parameters with varying values

Figure 1: Considered gravity column base-plate connection

Table 1: Parameters and considered values

Parameters	Considered values
Base plate thickness (t)	15, 25, 35 mm
Anchor rod diameter (d)	12, 16, 20 mm
Axial load (N)	40%ϕN_s (1425 kN), 60% ϕN_s (2273 kN)
Foundation depth (D)	1, 2 m
Anchor rod pitch distance (p)	50, 100, 150 mm

3 FINITE ELEMENT MODELLING

The connection has been modelled as a 3D finite element model using ABAQUS/CAE. First order-reduced integrated solid elements (C3D8R) were used for all components. Finer elements were used at locations where concentrated stresses are expected. The mesh sizes adopted were based on a prior mesh sensitivity analysis, conducted by the first author of this paper, such that the computational cost was minimized without scarifying the solution accuracy. Half of the connection was modelled, as only uni-directional load was applied.

3.1 Material modelling

All steel components were modelled with elastic and plastic material behaviour and the adopted standardized stress-strain relationships are shown in Figure 2. A Young's modulus (E) of 205 GPa was considered. The

column and base plate are AS/NZS 3679.1 (2016) Grade 300 and AS/NZS 3678 (2016) Grade 350 steel, respectively, where the anchor rods are AS/NZS 1110 (1995) Grade 4.6 steel which has a minimum yield strength (f_y) and minimum ultimate strength (f_u) of 240 MPa and 400 MPa, respectively. Finally, the nuts and anchor plate were defined as a perfectly elastic-plastic material with f_y = 350 MPa, while the washers were defined as an elastic material.

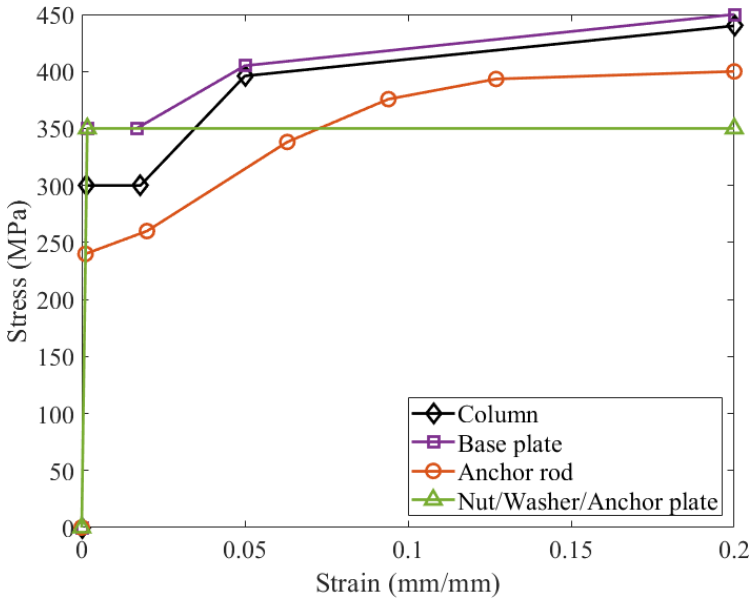

Figure 2: Adopted stress-strain relationships for the steel components

The grout and concrete foundation were modelled using the Concrete Damaged Plasticity (CDP) model in ABAQUS. The five required plasticity parameters for the CDP model are summarized in Table 2 following the validated recommendations provided by Shaheen et al. (2017). For the compressive behaviour, the concrete and grout have a compressive strength of 30 and 60 MPa, respectively. The stress-strain relationship of the concrete foundation was developed using the Hognestad's model (1955) where the stress-strain relationship of the grout layer was generated from Hsu and Hsu's empirical equations (1994). The tensile behaviour of the concrete and grout were defined with the stress - crack width relationship (Hillerborg et al., 1976) as it reduces possible convergence issues. The resultant compressive and tensile behaviours are shown in Figure 3.

Table 2: Adopted CDP model parameters

Parameters	Values
ψ	35
ϵ	0.1
σ_{b0}/σ_{c0}	1.16
K_c	0.667
μ	0.001

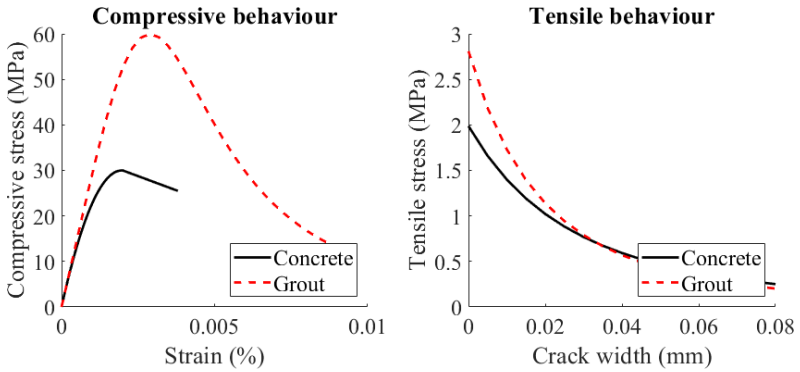

Figure 3: Adopted constitutive models for the concrete and grout

3.2 Contact modelling

The adopted contact modelling is shown in Figure 4. Hard contact was applied to all contact pairs in the normal contact direction. Separation after contact was allowed. Frictional contact was defined for the tangential contact direction. Specifically, a friction coefficient of 0.3 was applied to the grout-to-base plate contact as recommended by the HERA DCB No. 56 (2000). A friction coefficient of 0.5 was applied to all steel-to-steel contacts, as recommended by Ramhormozian (2018). A frictionless contact was assigned between the anchor rod and concrete foundation, as it was observed from an experimental study that the bond disappears quickly once the column is laterally loaded (Gomez et al., 2010). In addition, tie constraints were applied to the column-to-base plate, grout-to-concrete, nut-to-washer, and nut-to-rod surfaces to simulate strong connection.

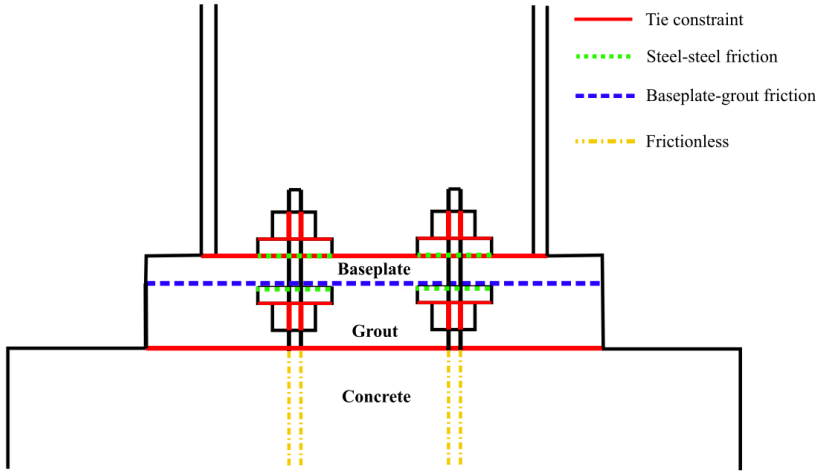

Figure 4: Adopted contact modelling for the column base-plate connection

3.3 Boundary conditions and loadings

Since soil flexibility is not considered, a fixed boundary condition was assigned to the base of the concrete foundation. Additionally, because only half of the connection was modelled, a symmetric boundary condition was assigned to the cross section of the model, fixing the out-of-plane displacement and rotation of the cross-sectional surface. The loadings on the model are applied in two steps. Compressive axial load was first applied as a pressure load on the top surface of the column. Once the axial load was fully applied, a displacement-controlled lateral loading was assigned to the top surface of the column, pushing the column to the target drift value, 5%.

3.4 Model validation

The developed finite element model was validated against experiments conducted by Gomez et al. (2010). Specifically, Test numbers 1, 4 and 5 were selected, as their test configurations captured the influence of base plate thickness, anchor rod strength and the presence of axial load. Figure 5(a) shows comparisons of the global responses (i.e., moment-column drift) of the connections where Figure 5(b) compares the local responses (i.e., anchor rod force-drift). Finally, Figure 5(c) compares the deformation profile of the base plate in Test 1. This comprehensive validation process avoids the developed model being "over-fitting", where there could be an excellent agreement of the global response but an inaccurate local response. Overall, the model results agree well with the experimental data.

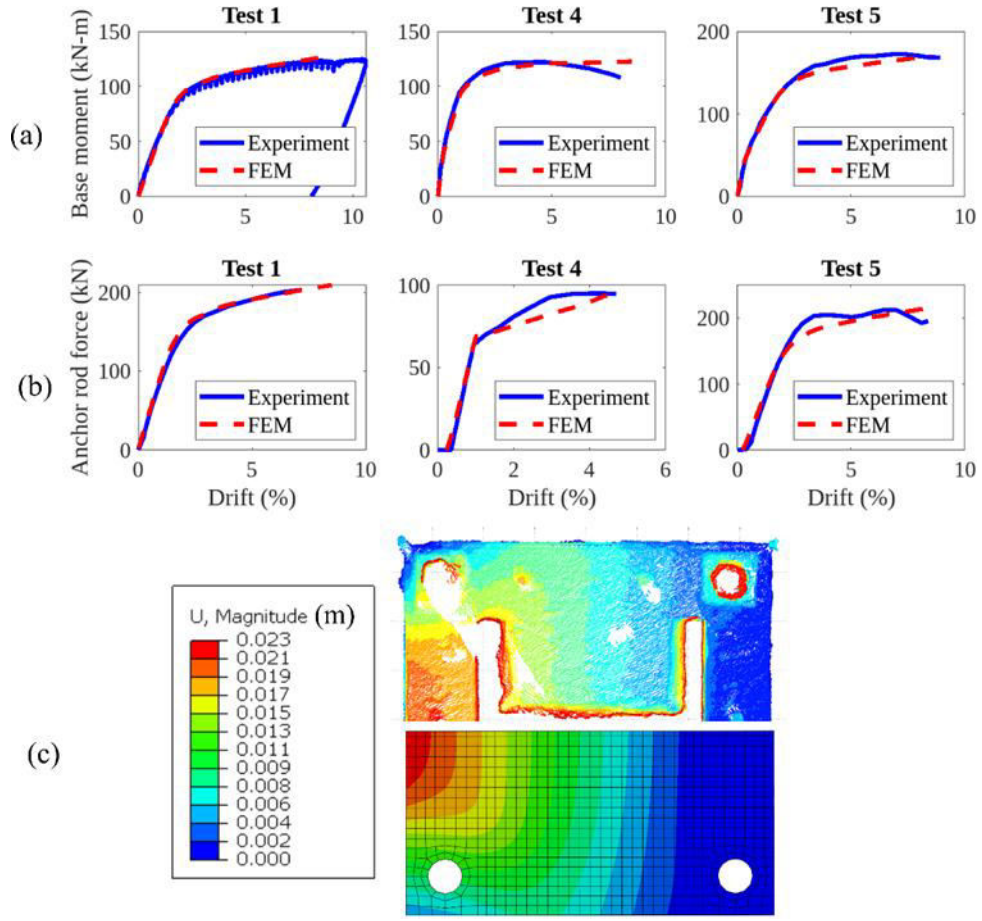

Figure 5: Model validation results. (a) Base moment-drift comparisons, (b) anchor rod-drift comparisons and (c) base plate deformation profile for Test 1

4 PARAMETRIC ANALYSIS RESULTS AND DICUSSIONS

This section presents the results from the numerical parametric analysis. It starts with the typical behaviour of the considered gravity column base-plate connection and is followed by discussions of the influence of each parameter on the connection rotational behaviour. Given that the adopted inflection point in this study was 0.6L from the base of the column, the column drift values used in the subsequent discussions were values from the finite-element analysis divided by 0.6 to approximate the drift at the column top.

4.1 Typical behaviour of the gravity column base-plate connection

The typical behaviour of the gravity column base-plate connection is shown in Figure 6. At the early stage of the loading, the moment at the column base increases linearly up to 0.35% column drift and then non-

linearity occurs. It should be noted that the non-linearity at this point is not due to yielding of the connection components, rather it is geometric non-linearity caused by partial lifting off of the base plate, as shown in Figure 6(a). This observation implies that the initial rotational behaviour of the connection is controlled by column compressing onto the base plate, grout layer and concrete foundation. Once the base plate is uplifted, the behaviour is then mainly governed by base plate bending and anchor rod elongation, which is significantly more flexible compared to the prior stage. At 1.2% column drift, the entire cross section of the anchor rod threaded portion has yielded, as shown in Figure 6(b), decreasing the stiffness of the connection. At 2.5% column drift, the entire cross section of the column flange yielded due to concentrated compression, as shown in Figure 6(c), further reducing the rotational stiffness of the connection. Finally, at 5% column drift (Figure 6(d)), the base plate starts to yield due to bending and localized compression.

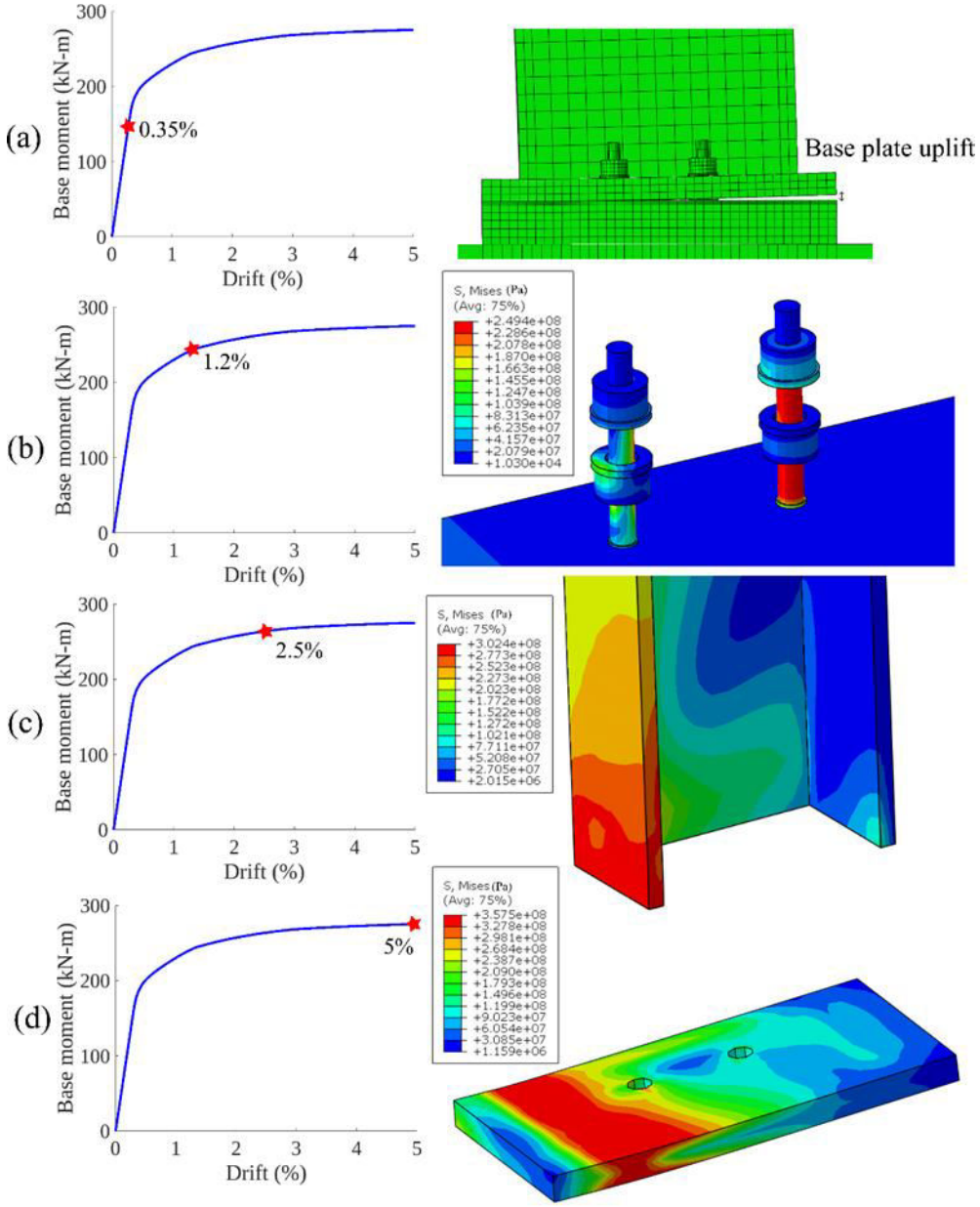

Figure 6: Typical pinned column base plate connection response. (a) Base plate uplift, (b) anchor rod yielding, (c) column flange yielding and (d) base plate yielding

4.2 Influence of the base plate thickness (t)

Figure 7 shows the influence of the base plate thickness on the connection moment-rotation behaviour. It was found that thicker base plates generate higher base moments. On average, the maximum base moment for connections with 35 mm base plate was approximately 9.8% and 4% higher than connections with 15 mm and 25 mm base plate, respectively. It was also observed that the base plate thickness had minimal effect at the early stage of the loading until the base plate was uplifted (i.e., when rotation reached above 0.7 mrads for this configuration).

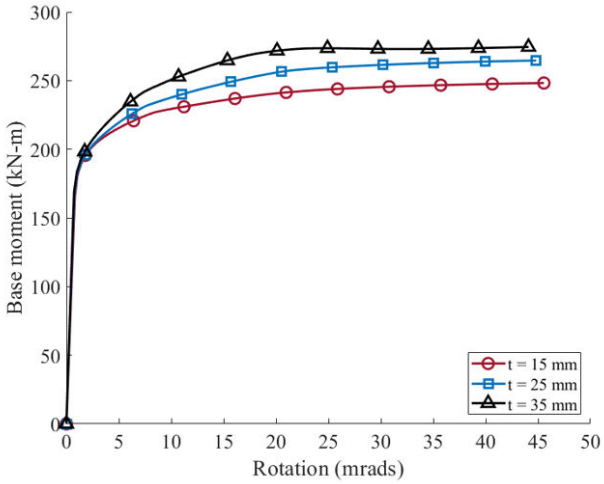

Figure 7: Influence of the base plate thickness on the moment-rotation behaviour

4.3 Influence of the anchor rod diameter (d)

The influence of the anchor rod diameter on the connection rotational behaviour is shown in Figure 8. It was observed that larger diameter rod results in greater base moment. On average, the maximum base moment for connections with 20 mm rod was approximately 13% and 5.8% higher than those connections with 12 mm and 16 mm rod respectively. The anchor rod diameter has minimal to no effect on the initial stage until the base plate is uplifted, where the anchor rods begin to stretch in tension and provide resistance.

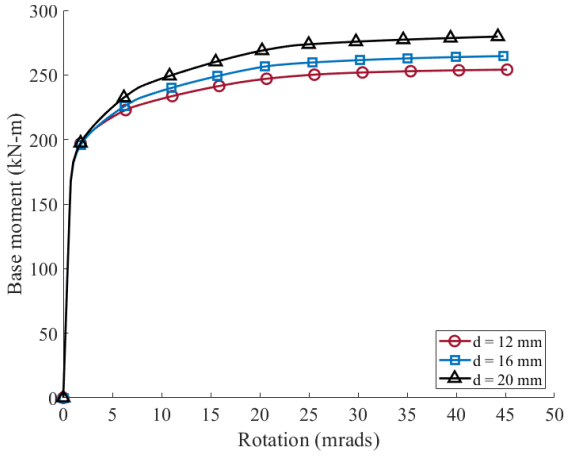

Figure 8: Influence of the anchor rod diameter on the moment-rotation behaviour

4.4 Influence of the foundation depth (D)

Figure 9 shows the effect of the foundation depth on the connection behaviour. It was found that a shallower foundation very slightly increases the base moment at around 5-10 mrads. This is due to the different axial stiffnesses caused by the different anchor rod embedment lengths. A shorter anchor rod embedment length results in a higher axial stiffness and hence provides higher resistance. However, the influence is insignificant. A considerable change in anchor rod embedment length (from 0.9 to 1.9 m) only leads to a change in base moment of less than 5%. Due to its insignificant effect, it was decided to exclude this parameter for the rest of the parametric study. However, if soil is included, the depth of the foundation would influence the stiffness of the foundation in soil and should not be neglected.

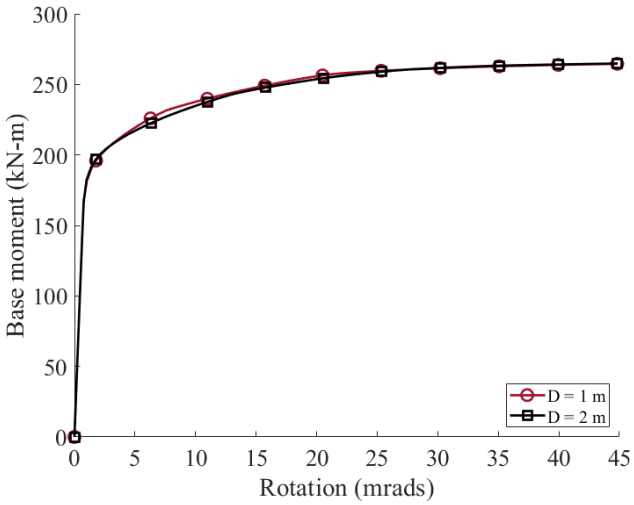

Figure 9: Influence of the foundation depth on the moment-rotation behaviour

4.5 Influence of the axial load ratio (N)

The influence of the axial load ratio is shown in Figure 10. It can be seen that higher axial load ratio significantly increases the base moment. This is because higher axial load provides greater uplift restraint, preventing the upward movement of the base plate. On average, the maximum column base moment for connections applied with $60\%\phi N_s$ were increased by 37% compared to connections with $40\%\phi N_s$. In addition, higher axial load delays the initiation of base plate uplift. Specifically, base plate uplift started at about 0.7 mrads for case N40 and 1.2 mrads for case N60. Figure 10 also shows the moment-rotation response for connection with no axial load. It was found that the initial stiffness was significantly lower as a result of the base plate being uplifted at the beginning of the loading stage. This observation further justifies the finding that the initial rotational stiffness is governed by the column flange compressing onto the base plate-grout-concrete assembly.

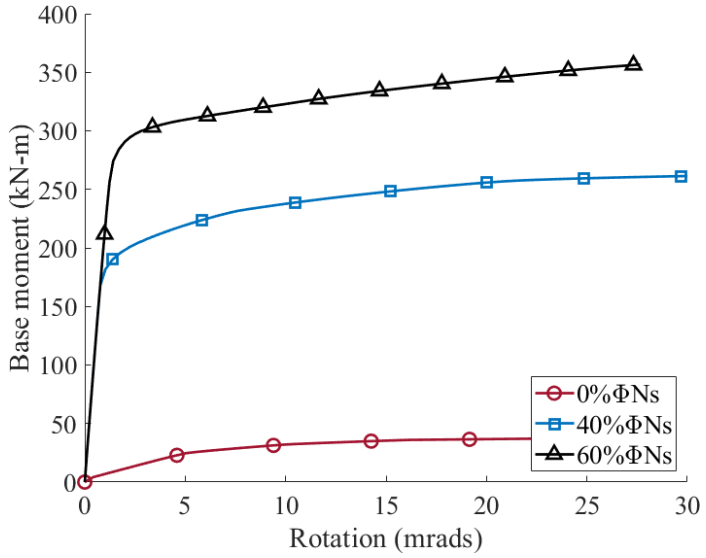

Figure 10: Influence of the axial load ratio on the moment-rotation behaviour

4.6 Influence of the anchor rod pitch distance (p)

The influence of the anchor rod pitch distance is shown in Figure 11. In general, a higher pitch distance leads to a slightly greater base moment. It is presumably due to the larger lever arm for the tension-side anchor rods. Overall, the effect of anchor rod pitch distance is minimal.

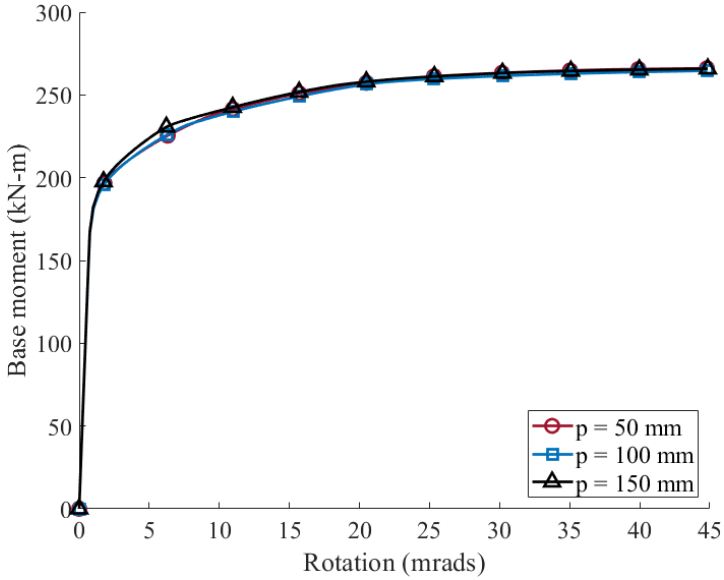

Figure 11: Influence of the anchor rod pitch distance on the moment-rotation behaviour

4.7 Influence of the considered parameters on the rotational stiffness

This section presents the influence of base plate thickness, anchor rod diameter and axial load ratio on the rotational stiffness. The foundation depth and anchor rod pitch distance both have neglectable effect on the connection behaviour and are therefore excluded. Given that the moment-rotation behaviour varies significantly throughout the loading history, three rotational stiffnesses were selected for comparison. These stiffnesses were taken at the serviceability limit state (SLS) drift, base plate-uplift drift and the ultimate limit state drift (ULS). The New Zealand Structural Design Actions Standard part 5, NSZ 1170.5 (2004), does not specify a single storey drift limit for SLS as it is based on the types of structure, claddings and partitions used. In this analysis, a drift limit of H / 400 (i.e., 0.25% drift), where H is the column height, was adopted. It

is one of the most widely used values based on ANSI/AISC 360 (2016). The base plate-uplift drift depends on the axial load, and as 0.35% and 0.55% were considered for $40\%\phi N_s$ and $60\%\phi N_s$, respectively. Finally, a drift of 2.5% was used for ULS as per NZS 1170.5 (2004). The rotational stiffnesses at these three drift limits are plotted in Figure 12. The y-axis on the left-hand side indicates the rotational stiffness in kN-m/mrads, whereas the right-hand side y-axis shows the rotational stiffness in the unit of EI/L. The x-axis indicates the values of the corresponding parameter. The following points were observed.

- The base plate thickness has the most pronounced influence on the rotational stiffness at low drifts (i.e., drifts prior to base plate uplift). It was observed that thicker base plates led to slightly higher initial rotational stiffness. On average, the initial rotational stiffness for case t35 is 13% and 4% higher than that for case t15 and t25, respectively. The variations are presumably caused by the base plate thickness which alters the compressive stress distribution under the base plate and therefore, affects the initial rotational stiffness of the connection. On the other hand, the anchor rod diameter and axial load ratio do not affect the rotational stiffness at low drifts.
- The applied axial load has the greatest influence on the rotational stiffness at high drifts (i.e., drifts after base plate uplift). It was found that the rotational stiffness for case N60 is on average 124% greater than that of case N40. The anchor rod diameter and base plate thickness also affect the rotational stiffness but at a much smaller rate. In particular, the rotational stiffness at ULS drift for case d20/t35 is on average approximately 11% and 5% higher compared to that for case d12/t15 and d16/t25, respectively.
- Figure 12 also plots the rotational stiffness for fixed and pinned bases (i.e., 1.67EI/L and 0.1EI/L, respectively) as per NZS 3404 (1997). It was found that the rotational stiffness for connections considered in this study (i.e., pinned connection) are much higher than the suggested limit, ranging from 0.4EI/L (at ULS drift) to 10EI/L (at SLS drift). The suggested value in NZS 3404 (1997) not only underestimates the actual rotational stiffness, but it is also incapable of reflecting the stiffness variation due to change of parameters. This comparison further shows that a method that could accurately calculate the connection rotational stiffness, considering the influences of the critical parameters, is needed. However, it is important to note that soil flexibility is not accounted for in this study, whereas the suggested rotational stiffness values in NZS 3404 (1997) aims to represent the realistic stiffness by including all influential parameters such as soil. That said, despite the significant underestimation observed from this analysis, the actual difference can only be determined when soil is considered in the analysis.

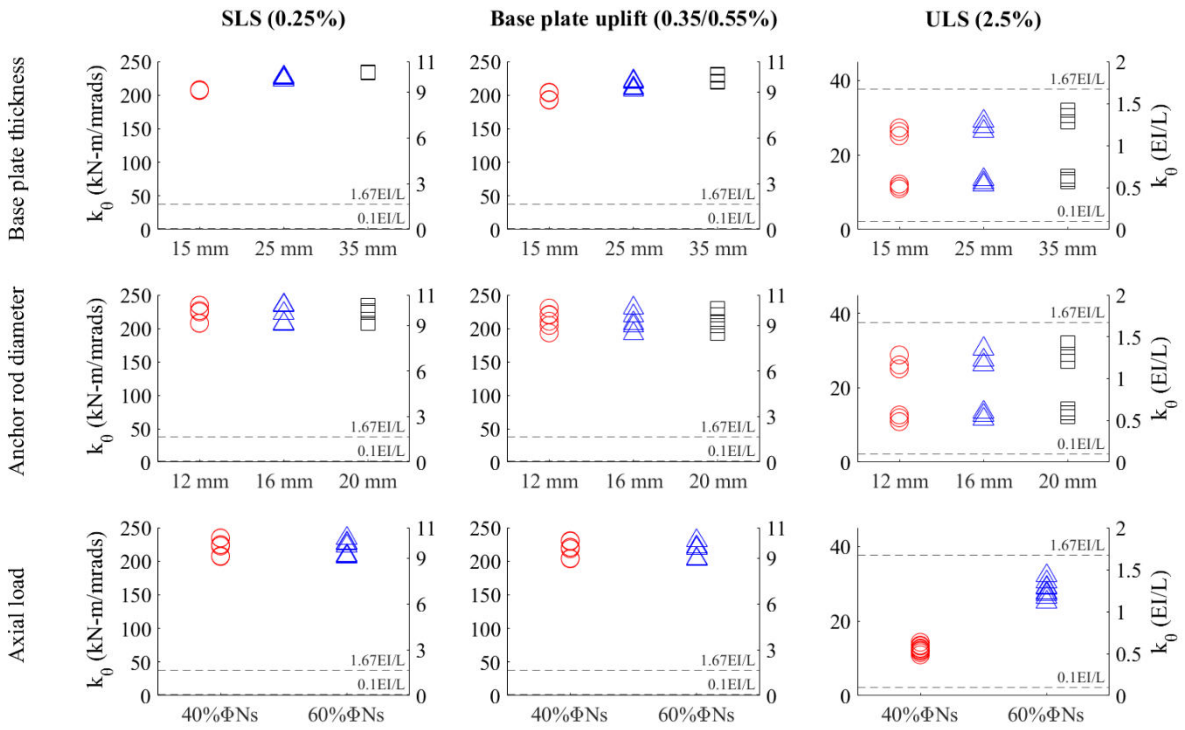

Figure 12: The effect of base plate thickness, anchor rod diameter and axial load ratio on the rotational stiffness

5 ONGOING RESEARCH – REVERSED CYCLIC ANALYSIS

This section presents ongoing research that expands on the parametric analysis. Rather than monotonic lateral loading, this analysis applies reversed cyclic lateral loading to the connection. The primary objective is to investigate the susceptibility of these pinned connections to axial shortening, specifically the initiation and the amount of shortening if it happens. For the finite element model, the column element was changed to shell element (S4R) and the full connection was modelled. This is to accurately simulate local and global column buckling which significantly contributes to axial shortening (Elkady & Lignos, 2018; MacRae et al., 2009). The same materials were used except with added cyclic hardening where needed. The base plate and column were modelled with the combined isotropic/kinematic hardening model (Lemaitre & Chaboche, 1990). The cyclic hardening parameters (i.e., Q_∞, b, C and γ), with one backstress, of the base plate was developed from the uni-axial tensile stress-strain data using the Constrained Optimization Approach proposed in de Castro e Sousa et al. (2021). The column's cyclic hardening parameters were developed and calibrated using the cyclic stress-strain response tested by Sinaie et al. (2014). To the best of the authors' knowledge, cyclic stress-strain data of Grade 4.6 rod is not available. Therefore, the anchor rods were modelled with the kinematic hardening model using the standard uni-axial tensile stress-strain curve and isotropic hardening was neglected. Cyclic hardening was not considered for washers, nuts and anchor plate. Table 3 summarizes the material properties for all steel components. In addition, two multi-linear rotational springs were assigned to the top of the column in the strong-axis direction to simulate realistic beam-column stiffness. The moment-rotation behaviour of these springs were developed based on Quan et al. (2022). Global and local imperfections in accordance with ASTM A6/A6M-13 (2003) and ASCE/SEI 7-16 (2016) were also assigned to the column. The full-model was validated by having the same result as the half-model, and the simulation of column buckling and shortening were validated using the experimental data from Elkady and Lignos (2018).

Table 3: Adopted cyclic hardening properties for the steel components

Components	Constitutive model	E (GPa)	σ_y (MPa)	Cyclic hardening parameters			
				Q_∞ (MPa)	b	C (MPa)	γ
Base plate	Combined isotropic/kinematic	205	321	168.3	2.86	2011	6.43
Column	Combined isotropic/kinematic	205	300	45.5	2	15800	147.5
Anchor rod	Kinematic	205	240				
Nut/anchor plate	Elastic perfectly plastic	205	350				
Washer	Elastic	205	350				

Table 4 summarizes the analysis conducted to date. One compact (310UC118) and one non-compact (310UC96) column section were selected. This is to investigate the influence of column cross section geometry on axial shortening, given that no specific column section category is required for the design of gravity columns. The configuration of the base-plate connection was designed in accordance to the SCNZ connection guide (2010) assuming that the column (310UC118) is loaded with a design axial load, 1.2G+1.5Q, equivalent 80% of the column section capacity (ϕN_s). The same base-plate configuration was used for all analysis cases to allow for direct comparison. The varying parameter in this analysis is the axial load ratio, ranging from high, 50% ϕN_s, to extreme loading, 60%ϕN_s. A symmetric uni-directional cyclic loading as per ref. (Krawinkler et al., 2000) was adopted in this analysis, as shown in Figure 13. Preliminary cyclic analysis of the connection showed that yielding of the first component, column flange at the base, occurred at around 0.75% column drift. Therefore, the number of cycles of 0.375% and 0.5% column drifts were reduced to one cycle in order to minimize computational cost. The maximum drift value is 3%, which is slightly above the ultimate limit state drift limit, 2.5%, outlined in NZS 1170.5 (2004). In terms of notations, letter C represents the column type and letter N represents the axial load ratio. Specifically, C1 is 310UC118 and C2 is 310UC96.

Table 4: Test matrix of the reversed cyclic analysis

ID	Column	Base plate dimension (mm)	Anchor rod diameter (mm)	Foundation depth (m)	Axial load (kN)	Pitch distance (mm)
		(d × b × t) [a]				
C1N60	310UC118 (compact)	450×450×36	20	0.89	2273 ($60\%\phi N_s$)	100
C1N50	310UC118 (compact)	450×450×36	20	0.89	1894 ($50\%\phi N_s$)	100
C2N60	310UC96 (non-compact)	450×450×36	20	0.89	2004 ($60\%\phi N_s$)	100
C2N50	310UC96 (non-compact)	450×450×36	20	0.89	1670 ($50\%\phi N_s$)	100

[a] Depth × width × thickness

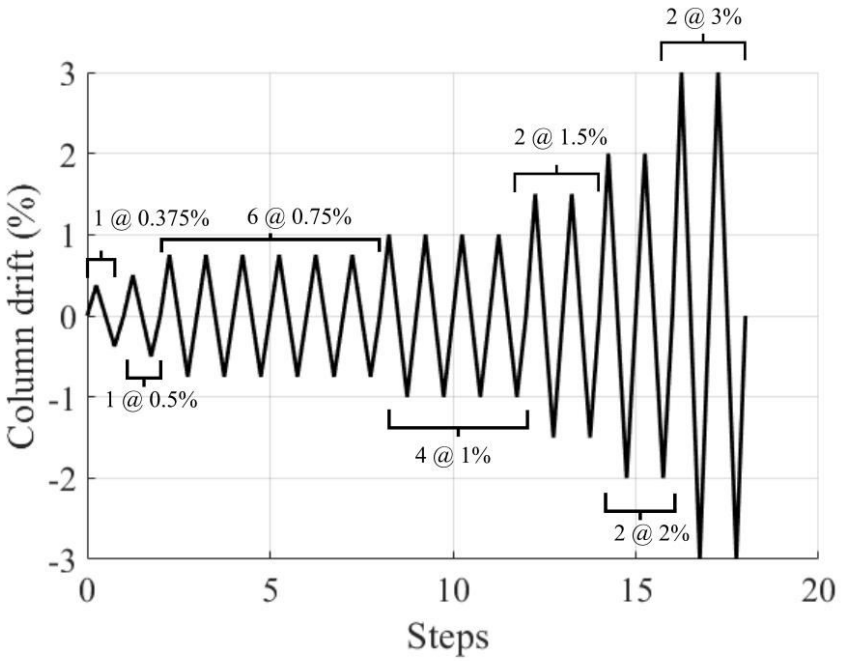

Figure 13: Symmetric reversed cyclic loading protocol

5.1 Results and discussions of the reversed cyclic analysis

Figure 14 shows the cyclic moment-drift response of the considered test cases. The connection behaviour for column C1 (310UC118) under load N50 and N60 are similar. As expected, the maximum base moment for case C1N60 is slightly higher compared to that of case C1N50 by 11% due to the greater applied axial load. Base plate uplift occurred at approximately 0.75% drift for both C1 cases which results in the first nonlinearity observed in the moment-drift responses. It is then followed by yielding of the bottom column flange occurred at 0.75% and 1% drift for C1N60 and C1N50, respectively. Finally, the anchor rods yielded at 1.5% drift for both C1 cases. It was also observed that the cyclic load paths followed the envelop curve (i.e,

the first-cyclic loading curve) closely, which is different from the results presented in Kavoura et al. (2017) and Pan et al. (2021). This is presumably due to the much higher axial load ratio applied in this cyclic analysis. On the other hand, the moment-drift response for case C2N60 (310UC96) differs significantly from that of C2N50. This is because the bottom of the column in C2N60 experienced severe buckling, as shown in Figure 15, which leaded to a progressive drop in base moment as the column drift increased. For case C2, base plate uplift and column flange yielding both occurred at 0.75% drift, and anchor rods yielded at 2% drift.

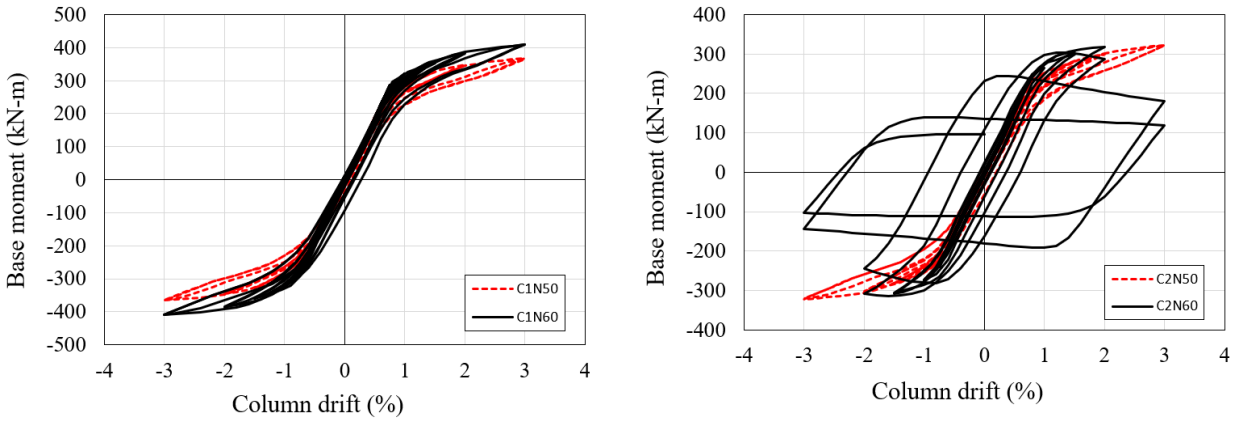

Figure 14: Cyclic moment-drift responses. Left hand side: compact column; right hand side; non-compact column

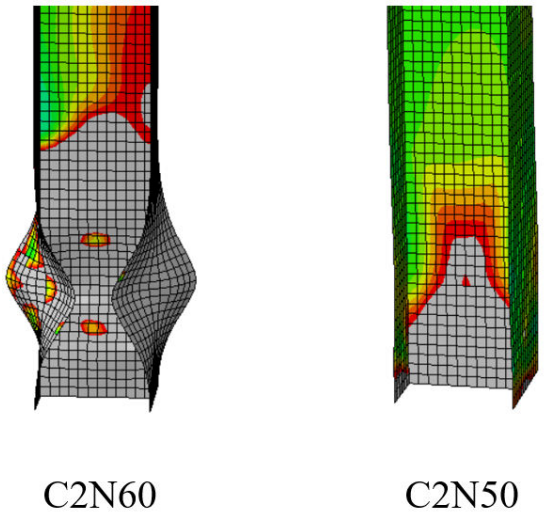

Figure 15: Column base profile (310UC96) at the end of the cyclic analysis

Figure 16 shows the amount of column axial shortening of the considered test cases. For case C1, the maximum shortening was 6.3 and 3.6 mm for load N60 and N50, respectively. It was found that shortening accelerated at about 1-1.5% drift, which was also the occurrence of column web yielding. There is a decrease in shortening for C2N50 when the column drift went from 0 to 3% drift. This is due to the combined effects of base plate uplift and the column being relatively less inelastic. For case C2, the maximum shortening was 46 and 4.7 mm for load N60 and N50, respectively. The significant shortening for C2N60 was again due to buckling at the column base, which initiated at around 1-1.5% drift. Elkady et al. (2019) conducted a survey to assess the repairability of steel columns that experience axial shortening. The survey shows that practical engineers in Japan and New Zealand are more on the conservative side, as their responses indicate a mean shortening limit of 10 mm, which may result in demolition when exceeded. Given the practical advice and

the results from the cyclic analysis, the authors suggest that the axial load demand during earthquake (i.e., G + Q_c) should be kept under 50%ϕN_s or a compact section (or both suggestions) should always be used for gravity columns.

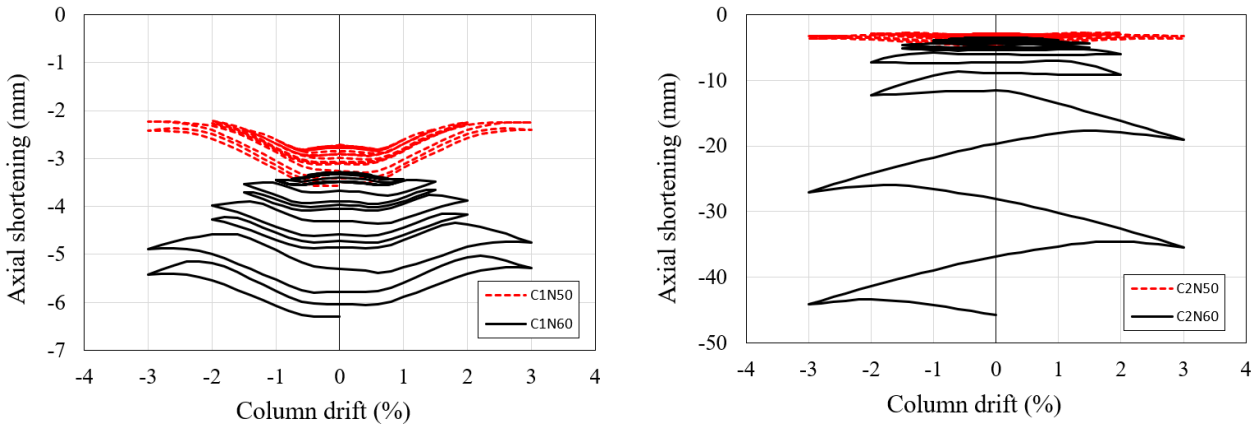

Figure 16: Axial shortening of the considered test cases. Left hand side: compact column; right hand side: non-compact column

6 CONCLUSIONS

Gravity column base-plate connections are normally treated as pinned connections with zero to little stiffness in practice. Past experimental and numerical studies showed that the rotational stiffness of these so-call "pinned" connections are much greater compared to the value provided in the New Zealand Steel Structures Design Standard. While the greater stiffness may seem beneficial, it attracts greater moment to the column and could potentially lead to yielding at the column base. In addition, the constant axial load applied on the yielded gravity column in conjunction with the seismic reversed lateral loading could facilitate axial shortening, which increases the cost and difficulty of post-earthquake rehabilitation. To further understand the realistic rotational stiffness of these gravity column base-plate connections, an extensive numerical parametric study (with ABAQUS/CAE 2021) was conducted to investigate the influences of the different parameters, including base plate thickness, anchor rod diameter, axial load magnitude, foundation depth and anchor rod pitch distance, on the connection behaviour. Furthermore, results from an ongoing work that focuses on the cyclic behaviour are also presented. The following conclusions are drawn from the analysis:

- The moment resistance of the connection generally increases with base plate thickness, anchor rod diameter and applied axial load. The depth of the foundation and anchor rod pitch distance considered in the study have insignificant effect on the moment resistance.
- The initial/pre-uplift rotational stiffness was found to be affected only by the base plate thickness presumably due to the changed in bearing area. However, such affect is minimal as a 130% increase in base plate thickness results in 13% increase in initial stiffness. The post-uplift stiffness was affected the most by axial load where an increase in moment of 124% was observed by increasing the axial load from 40%ϕN_s to 60%ϕN_s. The anchor rod diameter and base plate thickness also affect the post-uplift rotational stiffness but at a much smaller rate.
- Acknowledging the absence of soil flexibility in this analysis, the numerical results showed that the recommended stiffness value for pinned column base plate connections (i.e., 0.1EI/L) outlined in the New Zealand Steel Structures Design Standard significantly underestimates the actual rotational stiffness at all levels of column drift. Observations from the numerical analysis showed that the rotational stiffness was 4 to 100 times higher than the standard recommended

value. It is recommended that a more sophisticated approach to determining design column base rotational stiffness should be implemented rather than using a simplified form where the column geometry is the only influencing factor.

- The reversed cyclic analysis shows that a non-compact column, 310UC96, loaded with 60% of its design section capacity experiences severe buckling after cyclic loading that peaks that 3% drift. The resultant shortening was 46 mm. It is suggested that the axial load demand during earthquake should be kept under 50% of the column section capacity, or a compact section should always be used for gravity columns. Implementing both will give additional protection especially against the potential influence of biaxial bending which is being investigated in the next stage of this research.

ACKNOWLEDGEMENTS

The authors would like to thank the University of Auckland for providing the doctoral scholarship. The authors would also like to thank the New Zealand eScience Infrastructure (NeSI) for providing High Performance Computing (HPC) resources for the numerical parametric study. The support from New Zealand Ministry of Business, Innovation and Employment (MBIE) through an Endeavour Fund for the Research Programme (Sustainable Earthquake Resilient Buildings for a Better Future - PROP-83779-ENDRP-AUT) is greatly appreciated. Help from Late Professor Mick Pender and Professor Liam Wotherspoon from the University of Auckland and Kevin Cowie from the Steel Construction New Zealand (SCNZ) are also much appreciated.

REFERENCES

ANSI/AISC 360. (2016). *Specification for Structural Steel Buildings (ANSI/AISC 360-16)*. American Institute of Steel Construction, Chicago, Illinois.

ASCE/SEI 7-16. (2016). *Minimum design loads and associated criteria for buildings and other structures* (ASCE/SEI 7-16). Reston, VA: ASCE.

AS/NZS: 1110. (1995). *ISO metric precision hexagon bolts and screws*. Standards Australia; Standards New Zealand.

AS/NZS: 3678. (2016). *Structural steel-Hot-rolled plates, floor plates and slabs*. Standards Australia; Standards New Zealand.

AS/NZS: 3679.1. (2016). *Structural Steel Part 1: Hot-Rolled Bars and Sections*. Standards Australia; Standards New Zealand.

ASTM. (2003). *Standard specification for general requirements for rolled structural steel bars, plates, shapes, and sheet piling* (A6/A6M-13). West Conshohocken, PA: ASTM.

Borzouie, J., Chase, J. G., MacRae, G. A., Rodgers, G. W., & Clifton, G. C. (2016). Spectral assessment of the effects of base flexibility on seismic demands of a structure. *Advances in Civil Engineering*, *2016*, 1–8. https://doi.org/10.1155/2016/3984149

Clifton, G. C. (2000). Design concepts for moment-resisting column baseplate connections in a seismic-resisting system. *Design and Construction Bulletin (DCB)*, *HERA, No. 56*.

Clifton, G. C. (2013). Lessons learned for steel sesimic design from the 2010/2011 Canterbury earthquake series. *Australian Earthquake Engineering Society 2013 Conference*, Tasmania.

de Castro e Sousa, A., Hartloper, A. R., & Lignos, D. G. (2021). Cyclic Metal Plasticity Model Parameters with Limited Information: Constrained Optimization Approach. *Journal of Engineering Mechanics*, *147*(7), (ASCE)EM.1943-7889.0001922, 04021035. https://doi.org/10.1061/(ASCE)EM.1943-7889.0001922

Elkady, A., Güell, G., & Lignos, D. G. (2019). Proposed methodology for building-specific earthquake loss assessment including column residual axial shortening. *Earthquake Engineering & Structural Dynamics*, *49*(4), 339–355. https://doi.org/10.1002/eqe.3242

Elkady, A., & Lignos, D. G. (2018). Full-scale testing of deep wide-flange steel columns under multiaxis cyclic loading: Loading sequence, boundary effects, and lateral stability bracing force demands. *Journal of Structural Engineering*, *144*(2), 04017189. https://doi.org/10.1061/(ASCE)ST.1943-541X.0001937

Gomez, I., Kanvinde, A. M., & Deierlein, G. (2010). *Exposed column base connections subjected to aixal compression and flexure*. Final Report Presented to the American Institute of Steel Construction, Chicago.

He, J. C. W., Clifton, G. C., Ramhormozian, S., & Hogan, L. S. (2023). Numerical and analytical study of pinned column base plate connections [Manuscript under review]. *The University of Auckland*.

Hillerborg, A., Modéer, M., & Petersson, P.-E. (1976). Analysis of crack formation and crack growth in concrete by means of fracture mechanics and finite elements. *Cement and Concrete Research*, *6*(6), 773–781. https://doi.org/10.1016/0008-8846(76)90007-7

Hognestad, E., Hanson, N. W., & McHenry, D. (1955). Concrete stress distribution in ultimate strength design. *Journal Proceedings*, *52*(12).

Hsu, L. S., & Hsu, C.-T. T. (1994). Complete stress—Strain behaviour of high-strength concrete under compression. *Magazine of Concrete Research*, *46*(169), 301–312. https://doi.org/10.1680/macr.1994.46.169.301

Inamasu, H., Lignos, D. G., & Kanvinde, A. M. (2018). Effect of column base flexibility on earthquake-induced residual deformations of steel columns. *Key Engineering Materials*, *763*, 149–156. https://doi.org/10.4028/www.scientific.net/KEM.763.149

Kavoura, F., Gencturk, B., & Dawood, M. (2017). Reversed cyclic behaviour of column-to-foundation connections in low-rise metal buildings. *Journal of Structural Engineering*, *143*(9), 04017095. https://doi.org/10.1061/(ASCE)ST.1943-541X.0001821

Krawinkler, H., Gupta, A., Medina, R., & Luco, N. (2000). *Loading histories for seismic performance testing of SMRF components and assemblies* (SAC Joint Venture, SAC/BD-00/10). Richmond, CA.

Lemaitre, J., & Chaboche, J. L. (1990). *Mechanics of solid materials*. Cambridge, UK: Cambridge University Press.

MacRae, G. A., Urmson, C. R., Walpole, W. R., Moss, P., Hyde, K., & Clifton, C. (2009). Axial shortening of steel columns in buildings subjected to earthquakes. *Bulletin of the New Zealand Society for Earthquake Engineering*, *42*(4), 275–287. https://doi.org/10.5459/bnzsee.42.4.275-287

Nawar, M. T., Matar, E. B., Maaly, H. M., Alaaser, A. G., & El-Zohairy, A. (2021). Assessment of rotational stiffness for metallic hinged base plates under axial loads and moments. *Buildings*, *11*(8), 368. https://doi.org/10.3390/buildings11080368

Pan, J., Huang, R., Xu, J., Wang, P., Wang, Z., & Chen, J. (2021). Behavior of exposed column-base connections with four internal anchor bolts under seismic loading. *Structures*, *34*, 105–119. https://doi.org/10.1016/j.istruc.2021.07.016

Picard, A., & Beaulieu, D. (1985). Behaviour of a simple column base connection. *Canadian Journal of Civil Engineering*, *12*(1), 126–136. https://doi.org/10.1139/l85-013

Quan, G., Dai, X., Ye, J., Huang, S.-S., & Burgess, I. (2022). Modelling of composite fin-plate connections under fire conditions using component-based method. *Engineering Structures*, *264*, 114451. https://doi.org/10.1016/j.engstruct.2022.114451

Ramhormozian, S. (2018). *Enhancement of the Sliding Hinge Joint Connection with Belleville Springs*. Department of Civil and Environmental Engineering, PhD. thesis, The University of Auckland.

Shaheen, M. A., Tsavdaridis, K. D., & Salem, E. (2017). Effect of grout properties on shear strength of column base connections: FEA and analytical approach. *Engineering Structures*, *152*, 307–319. https://doi.org/10.1016/j.engstruct.2017.08.065

Sinaie, S., Heidarpour, A., & Zhao, X. L. (2014). Mechanical properties of cyclically-damaged structural mild steel at elevated temperatures. *Construction and Building Materials*, *52*, 465–472. https://doi.org/10.1016/j.conbuildmat.2013.11.042

Smith, M. (2021). *ABAQUS/Standard User's Manual* (Version 6.14). Providence (Rhode Island): Dassault Systemes Simulia Corp.

Standards New Zealand. (1997). *Steel structures standard (NZS 3404)*. NZS 3404: Part 1 & 2: 1997, New Zealand.

Standards New Zealand. (2004). *NZS 1170.5: 2004, Earthquake actions—New Zealand*. Standards New Zealand.

Steel Construction New Zealand. (2010). *Steel connect: Structural steelwork connections guide*. Steel Construction New Zealand.

Zareian, F., & Kanvinde, A. (2013). Effect of column-base flexibility on the seismic response and safety of steel moment-resisting frames. *Earthquake Spectra*, *29*(4), 1537–1559. https://doi.org/10.1193/030512EQS062M